Jetting regimes of double-pulse laser-induced forward transfer

Qingfeng Li, David Grojo, Anne-Patricia Alloncle, Philippe Delaporte

Research Article Vol. 9, No. 8 / 1 August 2019 / Optical Materials Express 3476
Optical Materials EXPRESS

Jetting regimes of double-pulse laser-induced forward transfer

QINGFENG LI,* DAVID GROJO, ANNE-PATRICIA ALLONCLE, AND PHILIPPE DELAPORTE

Aix-Marseille University, CNRS, LP3 laboratory, Campus de Luminy, 13009 Marseille, France
**li@lp3.univ-mrs.fr*

Abstract: We use the double-pulse laser-induced forward transfer (DP-LIFT) process, combining a quasi-continuous wave (QCW) and a femtosecond (fs) laser pulse to achieve jetting from a 1-μm thick copper film. The influence of the fs laser fluence on the dynamics of the liquid copper jetting is experimentally investigated by time-resolved shadowgraphy and theoretically analyzed with a simple energy balance model. Different jetting regimes are identified when varying the fs laser fluence. We demonstrate that the adjustment of this latter parameter while keeping all the others constant, allows accurate control of the diameter of the printed droplets from 1.9 μm to 6.0 μm. This leads us to a demonstration in which we print debris-free micro-pillars with an aspect ratio of 19 onto a silicon receiver substrate set as far as 60 μm away from the donor film.

1. Introduction

Laser-induced forward transfer (LIFT) of liquids is a nozzle-free printing technique that relies on the irradiation of a liquid film deposited on a donor substrate by a short laser pulse to initiate the motion of a small liquid volume, down to few picoliters, towards a receiver substrate. Experimental [1–5] and numerical [6–8] investigations on LIFT of liquid have been performed to identify the jetting mechanisms and to determine the optimum printing conditions. Whatever the configurations, LIFT without or with dynamic release layer [9,10], blister-actuated LIFT [11] or film-free LIFT [12], the laser irradiation induces a fast deformation of the film surface and the formation of a jet which expands away from the liquid donor to form a droplet on the receiver substrate. The main parameters that control the transfer process are the laser fluence, the film thickness and the liquid properties (density, surface tension or viscosity) [13]. The LIFT technique applied to liquids has been successfully used to print microdroplets with controllable diameters (down to 10 μm) and high reproducibility. It also provides new microfabrication opportunities in the fields of bio-engineering [14,15], optics [16] microelectronics [17] and sensors [18,19]. Moreover, with the motivation of addressing nanofabrication applications, laser-induced nano-jetting phenomena from solid donor films (< 1000 nm) has also been reported [20]. This was a subject of several experimental [21–26] and theoretical [27–29] studies. In that approach, an accurate combination of the film thickness, laser pulse duration, and energy allows with a single laser irradiation to both melt the whole film thickness and provide the relevant energy to deform the melted film and form the nanojet. Recently, different ejection regimes have been proposed [30,31] and the process has been used to fabricate high aspect ratio 2D/3D metal structures [32,33].

To further enlarge the processing windows and stabilize the transfer process, a double-pulse laser-induced forward transfer (DP-LIFT) technique has been recently proposed [34]. DP-LIFT process consists in irradiating a solid thin film deposited on a transparent carrier substrate by a first long-duration laser pulse, to locally melt the film, followed by a second irradiation with an ultrashort laser pulse to initiate the material transfer in liquid phase toward a receiver substrate. This method appears to be a versatile method to print high-resolution (< 2 μm) patterns with a long working distance (> 40 μm). It has successfully generated liquid nano-jets without debris

#363172 https://doi.org/10.1364/OME.9.003476
Journal © 2019 Received 26 Mar 2019; revised 7 Jun 2019; accepted 12 Jun 2019; published 25 Jul 2019

Optical Materials EXPRESS

from solid donor films of various materials (Cu, Au), leading to well-defined and clean printed structures [35,36].

In this paper, we investigate the influence of the fluence of the femtosecond laser on the dynamics of the transfer generated from the liquid copper film. Thanks to the time-resolved imaging experiments, jetting processes of the liquid copper are captured by high-resolution images series with 100-ns interval. By careful analysis of those high-quality images, jetting regimes induced by DP-LIFT from a 1-µm thick copper film are first identified. By varying the femtosecond laser fluence, different regimes, including the unique single droplet regime, are obtained. This study leads to an optimization of the DP-LIFT processing parameters that allows us to print copper droplets with controllable diameters ranging from 1.9 µm to 6.0 µm. Furthermore, debris-free micro-columns with aspect ratio as high as 19 are successfully printed, which brings DP-LIFT toward 3D microprinting applications.

2. Experimental setup

The experimental setup of DP-LIFT is presented in Fig. 1(a). For all the experiments presented in this paper, a 25-nm chromium interlayer was first magnetron sputtered onto a 1-mm-thick glass substrate as an interlayer to increase the adhesion. Then, a 1000-nm copper film is coated on this substrate as the donor. The laser with a long-duration pulse used to locally melt the donor film is a quasi-continuous wave (QCW) laser (IPG Photonics YLR-150/1500-QCW-AC-Y14). It emits at 1070-nm wavelength and delivers pulses of variable duration from 50 µs to the continuous wave operation. A femtosecond laser (Amplitude Systemes S-Pulse HP) emitting, at 515 nm wavelength (second harmonic), pulses of 500-fs duration (FWHM) is used to initiate the LIFT process. The femtosecond laser beam is focused at the center of the melted region to induce the material ejections. To do so, both beams enter collinearly through a long working distance Mitutoyo M Plan Apo 50 × (NA = 0.55) objective lens. The measured beam diameter at half maximum (FWHM) of the fs laser at the copper-donor interface is 1.6 µm. At the same location, the diameter of the QCW laser beam is measured at 9.7 µm. The femtosecond laser pulse energy is adjusted by the combination of a half-wave plate ($\lambda/2$) and polarized beam splitter (PBS). Time-resolved shadowgraphs of ejections are recorded using a CCD camera (QImaging QICAM) mounted on a customized microcopy arrangement based on a super-long working distance microscope objective lens (Mitutoyo M Plan Apo SL 50×, NA = 0.4). For time-resolved imaging, the flash source is provided by a nanosecond flash lamp (High-Speed

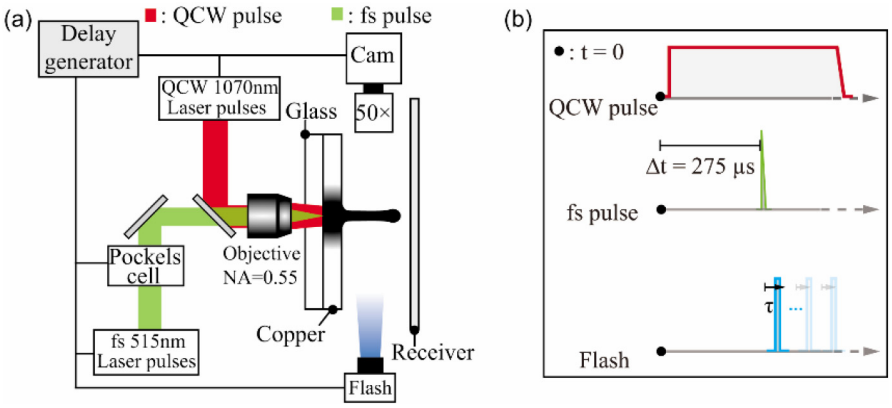

Fig. 1. (a) Sketch of the experimental setup for DP-LIFT. The QCW laser beam is in red, the femtosecond LIFT laser beam is in green, and the nanosecond flashlight is in blue. (b) Time chart for synchronization of the DP-LIFT and time-resolved observations.

Optical Materials EXPRESS

PHOTO-SYSTEME KL-M NANOLITE). The 12-ns duration of the flash determines the temporal resolution of the acquisition system. A digital delay generator (STANFORD RESEARCH SYSTEMS DG645) synchronizes, with adjustable delays, the triggering of the two lasers together with the flash illumination. In this study, a QCW laser pulse with a duration of 383 µs and a pulse energy of $770\mu J \pm 70\mu J$ is systematically applied. With this irradiation, after 150 µs, donor film starts melt from irradiation the center [36]. Even if such a long pulse is not needed to melt the whole film thickness, these conditions guarantee a clear separation between the slow melting process and the fast ejection process. Here, we arbitrary trigged the fs pulse with a fixed delay of 275 µs that ensures a constant diameter of the melted copper area [36]. The remaining energy delivered by the QCW pulse between 275 µs and 383 µs has no effect of ejection dynamics. After each femtosecond pulse irradiation, the flashlight illuminates the field-of-interest with a preset flash-to-LIFT delay τ. Thus, the ejection event with a delay of τ is captured by the camera.

3. Results and discussion

3.1. Jetting under different femtosecond laser fluences

We have shown in a previous work how the local temperature of the copper film can evolve from the room temperature to its vaporization point, and the corresponding molten pool diameter is changed during the irradiation by the QCW pulse. In the present investigations, we have chosen to deliver the femtosecond pulse with a fixed delay of 275 µs after the rising edge of the QCW pulse so that the molten pool diameter is always maintained at 20 µm and the temperature at the center of the molten pool is 1590 K according to calculations [36]. Under these conditions, liquid copper jetting behaviors induced by different femtosecond laser fluences are studied.

According to the time-resolved shadowgraphy observations, copper jetting is initiated by the motion of the liquid layer when the fs laser is applied. From the selected shadowgraphy images shown in Fig. 2, one can observe that the double-pulse LIFT induced copper jetting behaviors is similar to the case of single-pulse LIFT induced jetting from liquid donor films. As the velocity of the liquid is faster in the center of the beam, it leads to the formation of a liquid protrusion and initiates the jetting. The first results that we present here are related to the influence of the femtosecond laser fluence on the instantaneous ejection velocity of the protrusion. To describe this effect, the displacement of the ejection front is plotted as a function of τ, which is the delay between the fs laser and the flashlight (Fig. 2), and the slopes of the displacement curve provide directly the ejection velocities at different ejection moments. Figure 2(a) portraits the ejection event under a laser fluence ($\frac{pulse\ energy}{beam\ diameter\ area}$) of 8.0 J/cm^2. From the selected shadowgraphy captured at τ equals to 100 ns, 400 ns, and 700 ns, a general jetting process can be caught. At 100 ns, a protrusion has formed from the free surface; at 400 ns, this protrusion has shrunk and is about to pinch-off from the free surface; and at 700 ns, the ejection has escaped from the free surface and evolved into a spherical shape. Quantitatively, the plot of the ejection front displacement shows a deceleration process from $\tau = 100$ ns to $\tau = 400$ ns and the ejection velocity has decreased from 19.2 ± 5 m/s to 1.2 ± 1.0 m/s. Then, from $\tau = 400$ ns to $\tau = 600$ ns the jet starts to pinch-off from the free surface. After 600 ns, the ejected melt copper evolved into a spherical droplet and the displacement increases constantly. The constant velocity is measured as 16.5 ± 9.0 m/s. For a higher laser fluence of 10.3 J/cm^2, as portraited by the selected shadowgraphy images in Fig. 2(b), the ejection process is qualitatively similar to the low laser fluence case (8.0 J/cm^2). However, different ejection behaviors can also be observed especially for the image captured at $\tau = 700$ ns. Under the higher fluence, rather than evolving into a spherical shape, the ejected jet pinched from its middle and evolved into two spherical droplets. Quantitatively, from $\tau = 100$ ns to $\tau = 400$ ns the ejection velocity has also decreased from 40.1 ± 12 m/s to 4.1 ± 3.2 m/s. Then, from $\tau = 400$ ns to $\tau = 500$ ns the jet starts to pinch-off from the free surface. From $\tau = 500$ ns to $\tau = 700$ ns ejected jet will encounter a second pinching, and the displacement is oscillating

Optical Materials EXPRESS

during this period. After 700 ns, the jet evolved into two spherical droplets and the displacements increase constantly. The constant flying velocity is measured as 26.6 ± 3.3 m/s m/s. Finally, for a laser fluence of 30.0 J/cm^2, as portraited by the selected shadowgraphy images in Fig. 2(c), ejections exhibited different features under this high laser fluence condition. At $\tau = 100$ ns, the ejection is much faster and the velocity is measured as 83.7 ± 20 m/s. At $\tau = 400$ ns, compared to the two previous cases the jet has a much higher aspect ratio. And at $\tau = 700$ ns, the jet starts to encounter the end-pinching process and daughter droplet start to pinch-off from the jet end. However, despite those differences in comparison to the two previous conditions, it is striking to note the first pinching also occurs at $\tau \sim 450$ ns.

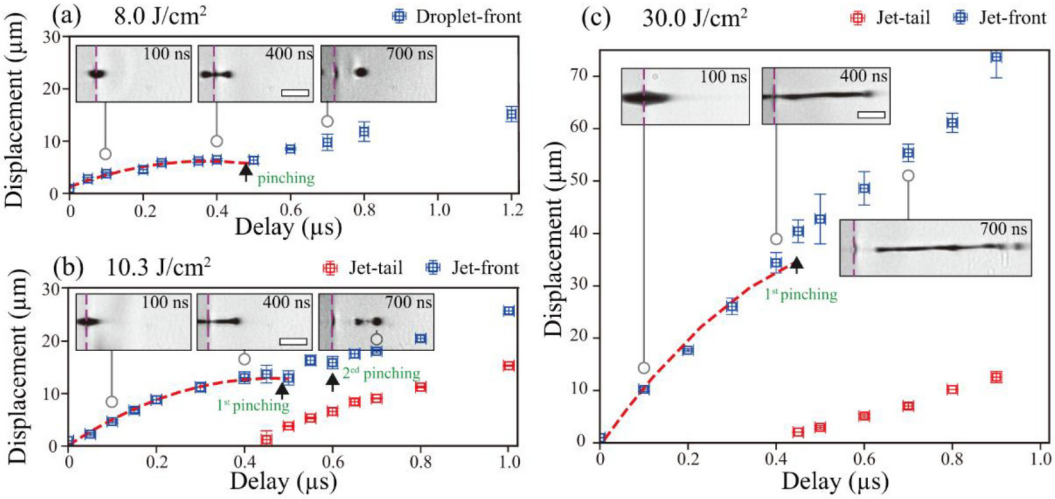

Fig. 2. Displacement evolutions of ejection fronts and tails induced under different femtosecond laser fluence: (a) 8.0 J/cm^2; (b) 10.3 J/cm^2; (c) 30.0 J/cm^2. Scale bar: 10 μm. The dash lines on the shadowgraphy images indicate the interface of donor and air. The jitter of the flash is approximately 20 ns, shown with the horizontal error bars on the data.

For further interpretation, the instantaneous ejection velocities at $\tau = 100$ ns for a large range of laser fluences are summarized in Fig. 3. They vary from 2.5 ± 0.5 m/s to 117.5 ± 10 m/s for femtosecond laser fluence varying from 7.3 J/cm^2 to 110.0 J/cm^2.

To understand this trend, an energy balance relation is considered. The conservation of the total energy (E_T) for the system of ejection can be written as:

$$\Delta E_T = \Delta E_k + \Delta E_s + \Delta E_d. \tag{1}$$

Since, we have only varied the femtosecond pulse energy in all experiments, an increase of the total energy ΔE_T is balanced by an increase of the kinetic energy $\Delta E_K = \frac{1}{2}\rho h_l A_{ej} V_{ej}^2$ and an increase of the surface energy $\Delta E_s = \gamma A_s$ or the conversion of heat through viscous dissipation ΔE_d. Here, ρ is the density, h_l is the height of the liquid column forming the jet, A_{ej} is the surface of the area where the ejection occurs, A_s the external surface of the jet and γ is the surface tension. We assume that the initial energy, which induced the deformation of the molten copper film and then the fluid motion, is provided by the vaporization of a small volume of copper at the interface with the transparent donor substrate when irradiated by the femtosecond pulse. This vapor energy is estimated to be equal to the incident laser energy minus the energy required for heating this volume up to the boiling temperature. Therefore:

$$\Delta E_T = E_{vap} = E_{abs} - A_{femto}(d_v L_m + d_v C_p (T_v - T)), \tag{2}$$

Optical Materials EXPRESS

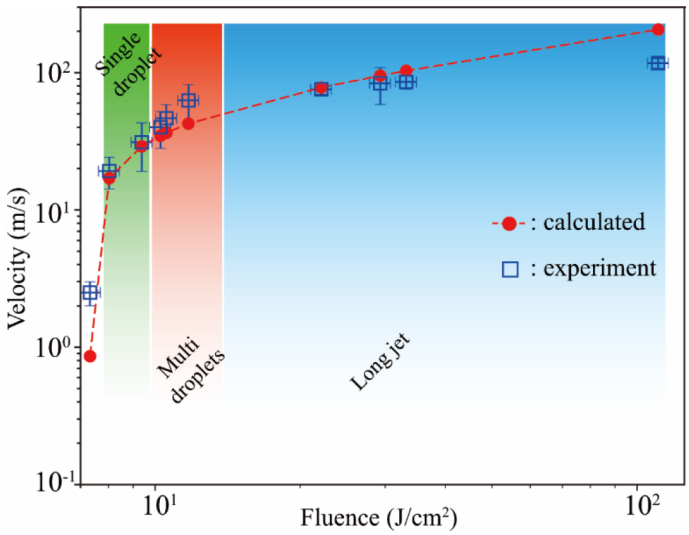

Fig. 3. Copper ejection velocity (measured at 100 ns) as a function of the femtosecond laser fluence. The different colored parts correspond to the different jetting regimes when the ejected material has traveled 50μm away from the donor surface. The blue squares are the measured values of the ejection velocity from the shadowgraphy experiments and the red dots represented the values of the velocity calculated thanks to the Eq. (3).

where E_{abs} is the femtosecond laser energy absorbed by the donor film, A_{femto} is the area irradiated by the femtosecond pulse, T is the temperature of the copper donor film when the fs pulse reaches its surface, d_v is the thickness of the vaporized donor, T_v is the boiling temperature of copper, C_p is the heat capacity of copper and L_m is the evaporation enthalpy of copper. Moreover, it is worth noting that, when calculating the E_{abs}, we have considered the chromium interlayer and use its reflectivity. However, since the chromium interlayer is only 25-nm thick, we ignored its contribution when calculating the heat capacity, surface tension and density.

As pointed out by Brown *et al* [5], during the early time of ejections ($\tau \leq 300$ ns) very little kinetic energy is viscously dissipated and the viscous dissipation ΔE_d is neglected in the following discussions. Then, by combining Eqs. (1) and (2), the ejection velocity is estimated:

$$V_{ej} = \sqrt{\frac{2CA_{femto}[F_{abs} - \rho d_v C_p(T_v - T)] - \gamma A_s}{\rho h_l A_{ej}}}. \tag{3}$$

The numerical values used to calculate V_{ej} are listed in Table 1. In order to estimate the ejection velocities with this simple model we did some assumptions. First, the surface of the laser spot A_{femto} and of the area where the ejection occurs A_{ej} have been experimentally measured for a fluence of 8 J/cm^2, and then A_{femto} and A_{ej} have been considered as constants when the fluence increases. As shown in Fig. 3, the good agreement between the experimental and calculated values of the velocities points out the small influence of A_{ej} for fluences lower than 30 J/cm^2 (see also Fig. 4 at delay of 100 ns). However, for fluences as high as 110 J/cm^2, A_{ej} can be four times higher than the constant value that we have used for the calculation. Therefore, under this fluence, the underestimation of A_{ej} leads to a significant difference between the calculated velocity and the experimental one.

Moreover, as discussed in the following section, the kinetic energy and the surface energy are very close near the fluence threshold while the kinetic energy becomes much higher than the surface energy when the fluence increases. For instance, at the fluence of 30 J/cm^2, based on the

Optical Materials EXPRESS

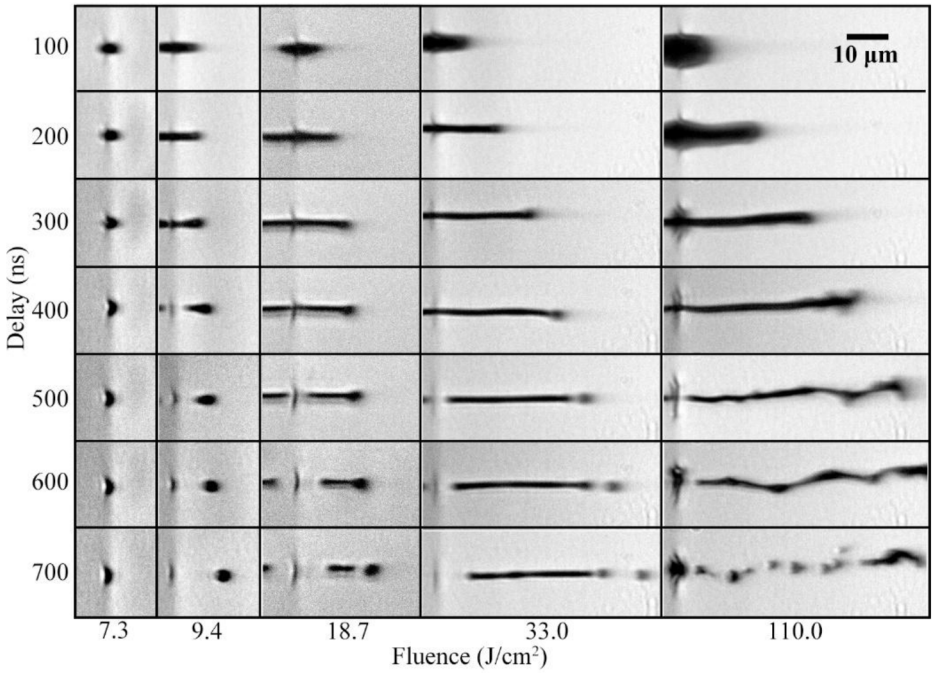

Fig. 4. Time-resolved shadowgraphy observations of ejections under different femtosecond laser fluences.

length, the diameter and the velocity of the jet measured at 100 ns after the fs laser irradiation, we estimated that the ratio of the kinetic energy over the surface energy is equal to 40. This means the surface energy term γA_s in the Eq. (3) can be neglected when the fluence is high enough. For simplicity reasons, we assumed that $A_s = A_{ej}$, and Fig. 3 shows that this assumption has no significant effect on the calculated V_{ej} when the laser fluence is higher than the ejection threshold. However, when this fluence becomes close to the ejection threshold, the discrepancy between the calculated and the measured velocity increases. In conclusion, these two assumptions appear to be valid in the range of fluences that is of interest for the printing applications.

Table 1. Numerical values used to calculate the ejection velocities from Eq. (3). We did not take into account the temperature dependence of these values.

A_{femto} (cm^2)	A_{ej} (cm^2)	ρ (kg/m^3)	L_m (J/kg)	C_p (J/kg·K)	d_v (nm)	γ ($J \cdot m^{-2}$)
2.0×10^{-8}	3.4×10^{-7}	7712	944 000	517	200	1.29

Here we assume that a fitting factor $C = 0.06$ is used for quantitative agreement. Similar fitting factor has also been reported by another group when investigating the vapor driven LIFT process [30]. In Ref. [30] researchers proposed this factor is due to a subtlety of the vaporization enthalpy, which partly consists of the energy required for the atom-by-atom escape through the liquid surface, and partly of the work done by the expanding vapor. Moreover, in our case, a shorter laser pulse is used which may also lead to the nonlinear absorption or even breakdown in the glass substrate. However, according to the time-resolved images presented in Fig. 4, the absence of the emitted white light from a potentially induced plasma near the glass-donor interface provides the indirect evidence of the limited nonlinear absorption in the glass substrate (if any). Nevertheless, a full understanding of the physical meaning of this factor would require further investigation. The numerical values obtained from Eq. (3) are reported in Fig. 3 and show a very

Optical Materials EXPRESS

good agreement with the experimentally measured velocities over a large range of fluences. This result suggests that our initial assumption on the origin of the film deformation, which is the vaporization of a small volume of copper at the donor/substrate interface, appears to be relevant.

3.2. Jetting regimes

In Fig. 4, we present time-resolved shadowgraph images of the ejections for different fluences (columns) with a frame-to-frame interval of 100 ns. First, at 7.3 J/cm^2, the ejection velocity at τ = 100 ns is measured as 2.5 ± 0.5 m/s, and the corresponding Weber number (i.e., the ratio of inertial energy and surface energy) is $We_{ej} = \frac{\rho d V_{ej}^2}{\gamma} \approx 0.08$. For such low Weber number, the kinetic energy of the liquid copper is not high enough to overcome the surface energy, and the material cannot detach from the donor film. This can be observed in the following frames of the first column as the protrusion is pulled-back to the free surface within 700 ns.

When the laser fluence is increased to 9.4 J/cm^2, the kinetic energy becomes high enough to overcome the pull-off force ($We_{ej} \sim 15$) and the liquid jet pinch-off from the free surface at $\tau \sim$ 400 ns. When this jet escapes from the free surface, it has an initial aspect ratio $L_0 \sim 4$ which rapidly evolves into a spherical spape. The Ohnesorge number, which represents the ratio of internal viscosity dissipation to the surface tension energy, of these liquid copper jets is equal to:

$$Oh = \frac{\eta}{\sqrt{\rho \gamma l}} \approx 10^{-2}, \tag{4}$$

where η is the liquid copper viscosity, ρ the density, γ the surface tension and l the jet diameter. Considering this initial aspect ratio and the Ohnesorge number, Notz *et al* [37] have simulated the evolution of the jet after the pinch-off, and their predictions confirm the formation of a spherical droplet. For a fluence of 18.7 J/cm^2, the pinch-off occurs at $\tau \sim 450$ ns and the initial aspect ratio is $L_0 \sim 10$. In this case, according to the prediction of Notz *et al* and our experimental observations, the jet can no longer evolves into an equilibrium spherical sphere but rather exhibits a series of complex oscillations before breaking in multiple droplets. At a fluence of 33.0 J/cm^2, the initial liquid protrusion has a higher aspect ratio, $L_0 \sim 19$, but the pinch-off still occurs at $\tau \sim$ 450 ns. Also as predicted [37], a so-called end pinching mechanism leads to the pinch-off of daughter drops from its ends during the afterward propagation. Further increase in fluence up to 110.0 J/cm^2, leads to the formation of the turbulent flow, which is not relevant to achieve reliable printing.

These results point out that the control of the fs laser fluence while keeping all the other parameters unchanged, allows varying first the morphology of the ejected materials, from single and multi-droplets to long liquid jets, and second the volume of transferred copper. In Fig. 3, we have reported the three observed regimes with different colors for guidance.

3.3. Printed microstructures

By placing a silicon substrate at 50 µm in front of the donor film, ejected materials can be collected. The DP-LIFT process is used to print 2D patterns of single pixels whose diameter is controlled by the laser fluence. Figure 5 presents the evolution of the sizes and the morphologies of the printed pixels for different fluences ranging from 8.2 J/cm^2 to 29.3 J/cm^2.

The first line of SEM images in Fig. 5 presents the deposits collected for a fs laser fluence of 8.2 J/cm^2, which corresponds to the jetting regime of a "single droplet". In this condition, the droplet diameter is 1.9 ± 0.15 µm. By slightly increasing the fluence to 8.8 J/cm^2, a single droplet with a larger diameter of 2.3 µm is printed (see the second line). With a laser fluence of 11.7 J/cm^2, the jetting occurs in the "multi droplets" regime. As shown in the third line of Fig. 5, the diameter of deposits further increased to 2.8 µm. By finally increasing the laser fluence to 29.3 J/cm^2, the jetting is located in the "long jet" regime and the diameter increased to 6.0 µm. As shown in the last line of Fig. 5(a), a first deposit is widely spread with a disk shape on the receiver surface,

Optical Materials EXPRESS

on which few smaller droplets are stacked. This indicates that during transfer the jet starts to pinch-off into daughter drops from its both ends. Those postmortem SEM analyses confirm the features of each jetting regime previously analyzed by means of time-resolved shadowgraph studies and the theoretical prediction of Notz *et al* [37]. Moreover, the droplets lines shown in Fig. 5(b) demonstrate the stability and reproducibility of DP-LIFT transfer over a large range of fs-pulse fluences. This could be of great technical significance for printing pixels over a wide range of dimensions without changing the donor film thickness. These results can be compared with those obtained by Feinaeugle et al. [38] when printing copper droplet with single pulse LIFT. They used a 6.7 ps pulse duration laser to print droplet with diameter ranging from 1 µm to 4 µm from a 200 nm thick solid film, by varying only the fluence, and they observed similar evolution of the droplet morphology when the fluence increases. However, such results can only be obtained in single pulse LIFT for a given thickness that depends on the pulse duration [31]. On the other hand, the use of double pulse LIFT allows the generation of stable liquid jet for a wide range of film thickness [20] and then a unique setup could print droplets with a large range of diameters by varying the fluence and the donor film thickness.

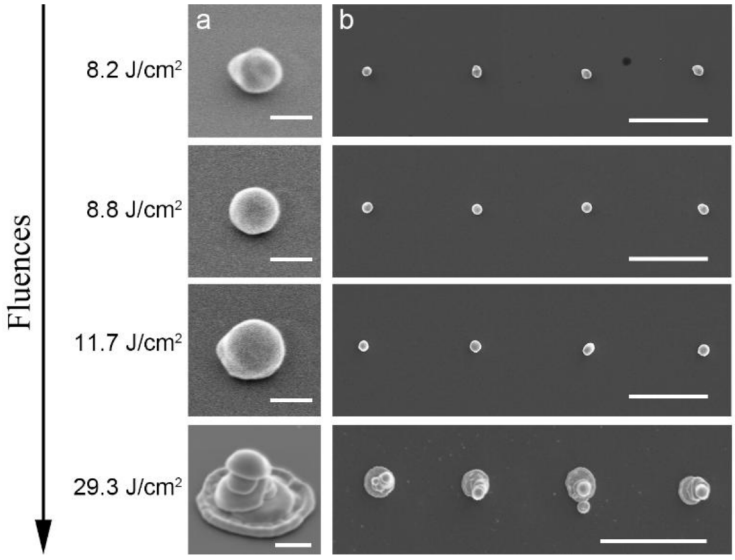

Fig. 5. Laser pulse fluence dependence of the micro-deposit diameter. (a) SEM angled views (50°) of droplets printed under different femtosecond laser fluences, scale bar: 2 µm. (b) SEM top views of droplet arrays, scale bar: 20 µm. The applied laser fluences (from 8.2 J/cm^2 to 29.3 J/cm^2) are the same for all droplets in each line.

At last, we demonstrate the ability of DP-LIFT for printing high aspect ratio metal microstructures. To do so, we selected the femtosecond laser fluence as 29.3 J/cm^2 to benefit from the feature of "long jet" regime and the formation of a relatively large base. Figure 6(a) presents an array of copper micro-pillars formed by three deposits. It is worth noticing that, even if those three deposits are initiated by the same laser conditions, their morphologies are not the same because of the different thermal conductivity for copper and silicon [39]. Indeed, when the first ejection reaches the silicon surface, liquid copper has enough time to spread out before getting solidified due to the relatively modest thermal conductivity of silicon, while when the jet reaches a copper surface it gets quickly solidified due to a higher thermal conductivity for copper. Finally, Fig. 6(b) shows a copper pillar with an aspect ratio of 19, and this pillar was built from nine stacked deposits. This last figure points out the potential of DP-LIFT for printing high aspect-ratio structures with a strongly limited amount of debris or satellites.

Optical Materials EXPRESS

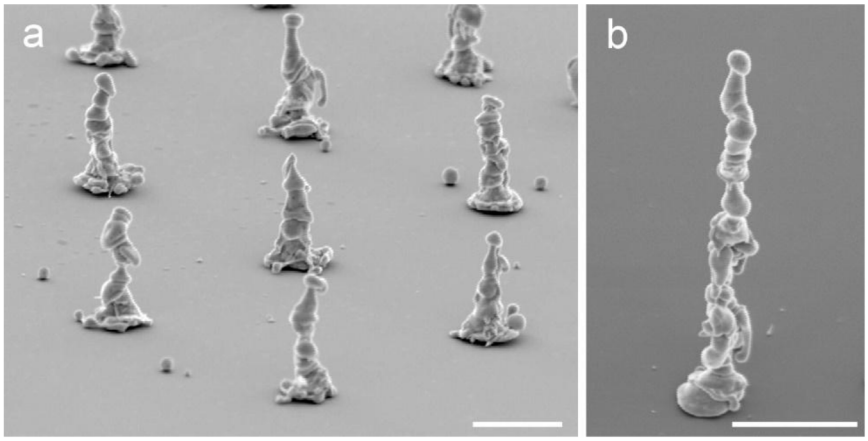

Fig. 6. 2.5D microstructures printed by DP-LIFT process. (a) SEM image of a micro-column array for which each column is stacked by three deposits, scale bar: 10 µm. (b) SEM image of a micro-column with an aspect ratio of 19 obtained by nine stacked deposits, scale bar: 10 µm.

4. Conclusions

Double pulse laser-induced forward transfer process, combining a quasi-continuous laser to locally melt a 1-µm thick solid copper film and a femtosecond laser to transfer the metal in the liquid phase, has been used to print copper structures with different morphologies while varying only the fs laser energy. An energy balance model has been used to predict the variation of the initial jetting velocity of liquid copper when the femtosecond laser fluence is varied. Time-resolved shadowgraph observations confirm the prediction of this model and this good agreement allows us to confirm that the driving mechanism of the initial fluid motion is the local ablation of a thin layer of the liquid copper by the fs pulse. These visualization studies also demonstrate that the different jetting regimes of those liquid metal jets are similar to those of other laser-induced liquid jets. Duocastella et al [2] has demonstrated that LIFT from 20 µm thick liquid donor allows printing debris free droplets with diameter ranging from 40 µm to 90 µm by varying the laser fluence. We observed a similar behaviour with a solid metal donor film when printing debris free droplets thanks to double pulse LIFT. Indeed, by varying the femtosecond laser fluence, while keeping all the other parameters constant, lines of droplets with pixel diameters from 1.9 µm to 6.0 µm have been successfully printed from a 1-µm thick solid film. That is an important result, because even if very impressive results have been obtained when printing metal in liquid phase from a solid film in single LIFT [38,40,41], that is difficult to fully get rid of satellites when the fluence is increased to print larger droplets. In terms of fabrication technology, we observed that the solidification process plays a significant role in the printed structure morphologies Micro-columns have also been fabricated with an aspect ratio up to 19 without significant debris. Taken together, all these results show the strong potential of this new approach for the development of a laser-based 3D additive manufacturing process at the microscale.

Funding

Agence Nationale de la Recherche (ANR) (ANR-16-CE08-0033); The Excellence Iniative of Aix-Marseille Université (AMU) - A*Midex, a French “Investissements d’Avenir” program.

Optical Materials EXPRESS

Acknowledgments

Authors sincerely acknowledge Professor Craig Arnold from Princeton University (Princeton Institute for the Science and Technology of Materials, Princeton University, Princeton, New Jersey 08544, USA) for his helpful comments and advice on the energy balance model.

References

1. C. B. Arnold, P. Serra, and A. Piqué, "Laser direct-write techniques for printing of complex materials," MRS Bull. **32**(1), 23–31 (2007).
2. M. Duocastella, J. M. Fernández-Pradas, J. L. Morenza, and P. Serra, "Time-resolved imaging of the laser forward transfer of liquids," J. Appl. Phys. **106**(8), 084907 (2009).
3. C. Boutopoulos, I. Kalpyris, E. Serpetzoglou, and I. Zergioti, "Laser-induced forward transfer of silver nanoparticle ink: time-resolved imaging of the jetting dynamics and correlation with the printing quality," Microfluid. Nanofluid. **16**(3), 493–500 (2014).
4. E. Biver, L. Rapp, A.-P. Alloncle, P. Serra, and P. Delaporte, "High-speed multi-jets printing using laser forward transfer: time-resolved study of the ejection dynamics," Opt. Express **22**(14), 17122–17134 (2014).
5. C. Unger, M. Gruene, L. Koch, J. Koch, and B. N. Chichkov, "Time-resolved imaging of hydrogel printing via laser-induced forward transfer," Appl. Phys. A **103**(2), 271–277 (2011).
6. C. Mezel, A. Souquet, L. Hallo, and F. Guillemot, "Bioprinting by laser-induced forward transfer for tissue engineering applications: jet formation modeling," Biofabrication **2**(1), 014103 (2010).
7. N. A. Inogamov, V. V. Zhakhovskii, and V. A. Khokhlov, "Jet formation in spallation of metal film from substrate under action of femtosecond laser pulse," J. Exp. Theor. Phys. **120**(1), 15–48 (2015).
8. M. S. Brown, C. F. Brasz, Y. Ventikos, and C. B. Arnold, "Impulsively actuated jets from thin liquid films for high-resolution printing applications," J. Fluid Mech. **709**, 341–370 (2012).
9. D. Karnakis, T. Lippert, N. Ichinose, S. Kawanishi, and H. Fukumura, "Laser induced molecular transfer using ablation of a triazeno-polymer," Appl. Surf. Sci. **127-129**, 781–786 (1998).
10. L. Rapp, A. K. Diallo, S. Nénon, A. P. Alloncle, C. Videlot-Ackerman, F. Fages, M. Nagel, T. Lippert, and P. Delaporte, "Laser printing of a semiconducting oligomer as active layer in organic thin film transistors: impact of a protecting triazene layer," Thin Solid Films **520**(7), 3043–3047 (2012).
11. N. T. Kattamis, P. E. Purnick, R. Weiss, and C. B. Arnold, "Thick film laser induced forward transfer for deposition of thermally and mechanically sensitive materials," Appl. Phys. Lett. **91**(17), 171120 (2007).
12. M. Duocastella, A. Patrascioiu, J. M. Fernández-Pradas, J. L. Morenza, and P. Serra, "Film-free laser forward printing of transparent and weakly absorbing liquids," Opt. Express **18**(21), 21815 (2010).
13. E. Turkoz, A. Perazzo, H. Kim, H. A. Stone, and C. B. Arnold, "Impulsively Induced Jets from Viscoelastic Films for High-Resolution Printing," Phys. Rev. Lett. **120**(7), 074501 (2018).
14. V. Dinca, A. Ranella, M. Farsari, D. Kafetzopoulos, M. Dinescu, A. Popescu, and C. Fotakis, "Quantification of the activity of biomolecules in microarrays obtained by direct laser transfer," Biomed. Microdevices **10**(5), 719–725 (2008).
15. J. A. Barron, P. Wu, H. D. Ladouceur, and B. R. Ringeisen, "Biological laser printing: a novel technique for creating heterogeneous 3-dimensional cell patterns," Biomed. Microdevices **6**(2), 139–147 (2004).
16. C. Florian, S. Piazza, A. Diaspro, P. Serra, and M. Duocastella, "Direct Laser Printing of Tailored Polymeric Microlenses," ACS Appl. Mater. Interfaces **8**(27), 17028–17032 (2016).
17. N. T. Kattamis, N. D. McDaniel, S. Bernhard, and C. B. Arnold, "Ambient laser direct-write printing of a patterned organo-metallic electroluminescent device," Org. Electron. **12**(7), 1152–1158 (2011).
18. F. Di Pietrantonio, M. Benetti, D. Cannatà, E. Verona, A. Palla-Papavlu, V. Dinca, M. Dinescu, T. Mattle, and T. Lippert, "Volatile toxic compound detection by surface acoustic wave sensor array coated with chemoselective polymers deposited by laser induced forward transfer: Application to sarin," Sens. Actuators, B **174**, 158–167 (2012).
19. C. Boutopoulos, E. Touloupakis, I. Pezzotti, M. T. Giardi, and I. Zergioti, "Direct laser immobilization of photosynthetic material on screen printed electrodes for amperometric biosensor," Appl. Phys. Lett. **98**(9), 093703 (2011).
20. Q. Li, D. Grojo, A. Alloncle, B. Chichkov, and P. Delaporte, "Digital laser micro- and nanoprinting," Nanophotonics **8**(1), 27–44 (2018).
21. Y. Nakata, N. Miyanaga, K. Momoo, and T. Hiromoto, "Solid-liquid-solid process for forming free-standing gold nanowhisker superlattice by interfering femtosecond laser irradiation," Appl. Surf. Sci. **274**, 27–32 (2013).
22. U. Zywietz, C. Reinhardt, A. B. Evlyukhin, T. Birr, and B. N. Chichkov, "Generation and patterning of Si nanoparticles by femtosecond laser pulses," Appl. Phys. A **114**(1), 45–50 (2014).
23. F. Korte, J. Koch, and B. N. Chichkov, "Formation of microbumps and nanojets on gold targets by femtosecond laser pulses," Appl. Phys. A **79**(4-6), 879–881 (2004).
24. J. P. Moening, S. S. Thanawala, and D. G. Georgiev, "Formation of high-aspect-ratio protrusions on gold films by localized pulsed laser irradiation," Appl. Phys. A **95**(3), 635–638 (2009).
25. C. Unger, J. Koch, L. Overmeyer, and B. N. Chichkov, "Time-resolved studies of femtosecond-laser induced melt dynamics," Opt. Express **20**(22), 24864–24872 (2012).

Optical Materials EXPRESS

26. D. Wortmann, J. Koch, M. Reininghaus, C. Unger, C. Hulverscheidt, D. Ivanov, and B. N. Chichkov, "Experimental and theoretical investigation on fs-laser-induced nanostructure formation on thin gold films," J. Laser Appl. **24**(4), 042017 (2012).
27. S. I. Anisimov, V. V. Zhakhovsky, N. A. Inogamov, S. A. Murzov, and V. A. Khokhlov, "Formation and crystallisation of a liquid jet in a film exposed to a tightly focused laser beam," Quantum Electron. **47**(6), 509–521 (2017).
28. N. A. Inogamov, V. V. Zhakhovsky, V. A. Khokhlov, Y. V. Petrov, and K. P. Migdal, "Solitary Nanostructures Produced by Ultrashort Laser Pulse," Nanoscale Res. Lett. **11**(1), 177 (2016).
29. N. A. Inogamov, V. V. Zhakhovskii, and V. A. Khokhlov, "Jet formation in spallation of metal film from substrate under action of femtosecond laser pulse," J. Exp. Theor. Phys. **120**(1), 15–48 (2015).
30. R. Pohl, C. W. Visser, G. W. Römer, D. Lohse, C. Sun, and B. Huis in 'T Veld, "Ejection regimes in picosecond laser-induced forward transfer of metals," Phys. Rev. Appl. **3**(2), 024001 (2015).
31. M. Zenou, A. Sa'ar, and Z. Kotler, "Laser jetting of femto-liter metal droplets for high resolution 3D printed structures," Sci. Rep. **5**(1), 17265 (2015).
32. C. W. Visser, R. Pohl, C. Sun, G. W. Römer, B. Huis in 't Veld, D. Lohse, B. Huis In 'T Veld, and D. Lohse, "Toward 3D Printing of Pure Metals by Laser-Induced Forward Transfer," Adv. Mater. **27**(27), 4087–4092 (2015).
33. M. Zenou and Z. Kotler, "Printing of metallic 3D micro-objects by laser induced forward transfer," Opt. Express **24**(2), 1431–1446 (2016).
34. Q. Li, A. P. Alloncle, D. Grojo, and P. Delaporte, "Generating liquid nanojets from copper by dual laser irradiation for ultra-high resolution printing," Opt. Express **25**(20), 24164–24172 (2017).
35. Q. Li, A. P. Alloncle, D. Grojo, and P. Delaporte, "Laser-induced nano-jetting behaviors of liquid metals," Appl. Phys. A **123**(11), 718 (2017).
36. Q. Li, D. Grojo, A.-P. Alloncle, and P. Delaporte, "Dynamics of double-pulse laser printing of copper microstructures," Appl. Surf. Sci. **471**, 627–632 (2019).
37. P. K. Notz and O. A. Basaran, "Dynamics and breakup of a contracting liquid filament," J. Fluid Mech. **512**, 223–256 (2004).
38. M. Feinaeugle, R. Pohl, T. Bor, T. Vaneker, and G. W. Römer, "Printing of complex free-standing microstructures via laser-induced forward transfer (LIFT) of pure metal thin films," Addit. Manuf. **24**, 391–399 (2018).
39. A. I. Kuznetsov, R. Kiyan, and B. N. Chichkov, "Laser fabrication of 2D and 3D metal nanoparticle structures and arrays," Opt. Express **18**(20), 21198–21203 (2010).
40. D. P. Banks, Ch. Grivas, J. D. Mills, and R. W. Eason, "Nanodroplets deposited in microarrays by femtosecond Ti:sapphire laser-induced forward transfer," Appl. Phys. Lett. **89**(19), 193107 (2006).
41. M. Zenou, A. Sa'ar, and Z. Kotler, "Digital laser printing of aluminum microstructure on thermally sensitive substrate," J. Phys. D: Appl. Phys. **48**(20), 205303 (2015).